2024 33rd International Conference on Computer Communications and Networks (ICCCN) | 979-8-3503-8461-1/24/$31.00 ©2024 IEEE | DOI: 10.1109/ICCCN61486.2024.10637648

ECG-grained Cardiac Monitoring Using RFID

Ningning Wang[†], Tianya Zhao[†], Shiwen Mao[‡], Harrison X. Bai[∓], Zhicheng Jiao[±], Xuyu Wang[†]
[†]Knight Foundation School of Computing and Information Sciences, Florida International University, Miami, FL 33199
[‡]Department of Electrical and Computer Engineering, Auburn University, Auburn, AL 36849-5201
[∓]Department of Radiology and Radiological Science, Johns Hopkins University School of Medicine, Baltimore, MD 21287
[±]Department of Diagnostic Imaging, Rhode Island Hospital, Providence, RI 02903
Emails: {nwang012, tzhao010}@fiu.edu, smao@ieee.org, hbai7@jhu.edu, zhicheng_jiao@brown.edu, xuywang@fiu.edu

***Abstract*—Heartbeat signals are useful to disease prediction, sub-health diagnosis, fatigue warning, and even emotion estimation. There is a compelling need for contactless, easy-to-deploy, and long-term heartbeat monitoring. This paper presents a contactless Radio Frequency Identification (RFID) based system for heartbeat monitoring that leverages the insight that RFID signal fluctuations induced by chest motion are synchronous with both respiration and heartbeat. The proposed system collects the temporal phase information from the tag pair on the body to extract heartbeat signals using a sequence of signal processing techniques. We propose a signal separation method based on empirical mode decomposition (EMD) to obtain heart rate after preprocessing. Furthermore, the estimated signal is input to an enhanced variational autoencoder (VAE) model to recover the heartbeat waveform. Implemented with commercial off-the-shelf (COTS) RFID devices, the system achieves accurate heart rate monitoring with less than 3% relative errors. The detected waveform exhibits a median cosine similarity of 0.83 as compared with the ground truth, which validate the system's wide applicability and high reliability for fine-grained, contactless heartbeat monitoring.**

***Index Terms*—Radio Frequency Identification (RFID), vital sign monitoring, contact-free sensing, variational autoencoder.**

I. Introduction

Vital signs such as respiration rate and heart rate are fundamental physiological parameters for health diagnosis and monitoring general well-being. Traditionally, techniques such as Photoplethysmography (PPG) and Electromyography (EMG) have been widely used for monitoring heartbeat signals [1], [2]. However, both methods require expensive, heavy, and power-consuming equipment that is inconvenient for continuous daily use, especially during sleep. As a result, there is a growing demand for contactless vital sign monitoring solutions from both academia and industry to enable non-invasive long-term tracking of vital signs.

By leveraging the selected signals to capture body micro-movements, contactless sensing provides a promising means to monitor vital signs. Among the research in recent years, several wireless techniques have been studied for monitoring heartbeat, including radar [3], Wi-Fi [4], acoustics [5], and camera [6], etc. Some of the wireless systems depend on expensive or dedicated equipment that uses a large bandwidth, such as ultra-wideband (UWB) radar [7] and frequency modulated continuous wave (FMCW) radar [8], which has been a hindering factor to their large-scale deployment and long-term use. Some devices are dependent on the environment and they need a line-of-sight (LOS) path to obtain accurate measurements, such as Zigbee [9].

In contrast, Radio Frequency Identification (RFID) systems can mitigate the impact caused by multiple users as well as multi-path propagation, where the RFID reader receives signals reflected from passively tags to obtain information about the target for different Internet of Things (IoT) sensing applications (e.g., localization, action recognition, and vital sign monitoring). In addition, the tags are small, low-cost, and battery-free, making them to be easily and unobtrusively deployed to users. Furthermore, their nature of identification can be used to effectively and easily distinguish different human subjects. In this paper, we exploit the backscattered RFID signal modulated by the chest motion caused by respiration and heartbeat. We show that the commercial off-the-shelf (COTS) RFID is adequate for monitoring heartbeat because its reading rate per tag (almost 50 Hz) is much higher than the normal heart rate ($50 \sim 90$ beats per minute (bpm) [10]) for a healthy adult at rest. Zhao *et al.* [11] have succeeded in implementing a multi-tag empirical mode decomposition (EMD) method to detect heartbeat from the RFID phase. Wang *et al.* also utilize wavelet transform to extract the heartbeat from RFID signals [12]. Although the rationale behind such works sounds fairly intuitive, it is still challenging to monitor both respiration and heartbeat reliably and robustly, becuase

1) COTS RFID devices, due to inherent limitations in their configuration, have the problem caused by frequency hopping, i.e., their interrogation frequencies rapidly and randomly hopping among multiple channels during communication with tags.
2) Small movements of the chest cavity caused by heartbeat signals are difficult to capture due to the relatively larger body movements associated with unconscious body movements and respiratory activity of the subject.
3) Heartbeat signal obtained indirectly through chest movements are quite different from that detect by accurate medical electrocardiogram (ECG) equipment, while the latter is more useful from the medical perspective.

In this paper, we leverage two COTS RFID tags to set up an RFID heartbeat monitoring system, which aims to recover the heartbeat signal with similar accuracy as that from traditional ECG devices. Due to the sampling frequency of RFID system, we can ensure the same frequency of interrogation for both tags

within a short period of time, and the difference between their phases will only contain the movement signals of the subject. Thus the influence of frequency hopping can be mitigated.

To deal with the impact of body movements, we utilize one of the tags as a reference tag, through which to construct a relative coordinate system. Specifically, we attach two COTS RFID tags to the chest area of the human subject. One is attached near the chest cavity and the other near the collarbone. A COTS RFID reader is used to continuously interrogate these tags by issuing a continuous wave and collecting their backscattered RF signals within the effective scanning range ($0.25 \sim 1$m). We utilize the readily available measured RFID phase data to extract the rhythmic pattern associated with heartbeat. Similar to traditional testing methods, the environment is controlled to be relatively quiet and the test subjects are supposed to remain still during the measurement.

Generally, heartbeat waveform is considered significantly more useful than heartrate, as it depicts the entire cardiac cycles with much richer information [13]. To detect the heartbeat waveform from the RFID signal, we propose using a variational autoencoder (VAE) with an enhanced loss function. In particular, the traditional loss function contains only the mean square error (MSE) derived relative to the ground truth but ignores the physical boundaries in the experiment. Therefore, better performance can be achieved by adding physical constraints to the loss function.

The main contributions made in this paper include:

1) To the best of our knowledge, this is the first work that harnesses the COTS RFID system to monitor the heartbeat waveform. Compared to traditional methods, we obtain waveforms that approximate ECG signals by utilizing a series of signal processing techniques coupled with a deep learning model.
2) We also propose a novel technique to deal with the frequency hopping offset, which is a phase difference calibration method. The proposed scheme is simple but effective in mitigating the frequency hopping offset as well as constructing a relative coordinate system to eliminate the effects of other body movements and displacements.
3) In order to estimate the heartbeat waveform, a method of using a modified VAE with physically bounded loss function is proposed.
4) We implement the system with COTS RFID devices, which can obtain accurate heart rate monitoring with less than 3% relative errors. The recovered waveform shows a median cosine similarity of 0.83 compared with the ground truth.

The remainder of this paper is organized as follows. Section II provides the preliminaries and motivation. The proposed system design is presented in detail and analyzed in Section III. The experimental study is discussed in Section IV. Section V concludes this paper.

II. Preliminaries and Motivation

In this section, we will first introduce the frequency hopping problem, which is a key issue that appears in all RFID research. It is caused by the regulations of the Federal Communications Commission (FCC) in the interest of communications security. Then, we explain the rationale of contact-free cardiac monitoring. We will establish the connection between the physical phenomenon of heartbeat and the phase of RF signal, and deduce how to obtain the heartbeat signal. After that, the principle and a feasibility analysis of heartbeat monitoring via RF signals will be presented.

A. Frequency Hopping

Under the requirements set by the FCC, in order to prevent co-channel interference, ultra high frequency (UHF) RFID readers need to adopt a channel hopping strategy. The spectrum, from 902.5 MHz to 927.5 MHz, has been divided into 50 non-overlapping channels. According to the regulations, the reader should occupy every allocated channel for 200 ms before transitioning to the subsequent channel. Although this regulation improves communication robustness and security, it introduces an additional phase shift in the RFID signal, which can lead to significant inaccuracies in RFID-based measurements and sensing.

According to the official RFID reader manual [14], the phase ϕ of the received RFID response signal can be expressed as

$$\phi = \mathrm{mod}\left(\frac{4\pi\ell}{\lambda} + \sigma_T + \sigma_R + \sigma_{Tag}, 2\pi\right), \tag{1}$$

where ℓ is the distance between the tag and reader antenna, λ is the wavelength of the current interrogation signal, σ_T, σ_R and σ_{Tag} are phase offsets caused by the transmitter circuit, receiver circuit, and tag's reflection characteristics, respectively.

Channel hopping causes the ϕ to change as the wavelength of the interrogation signal changes, even if the distance remains constant. In addition, wavelength is not the only factor that causes the phase change. σ_T, σ_R and σ_{Tag} are the phase offsets irrelevant to the distance ℓ, which are also influenced by the channel frequency. We rewrite (1) as follows:

$$\phi(f_i, \ell) = \mathrm{mod}\left(\frac{4\pi f_i \ell}{c} + \sigma_i, 2\pi\right), \tag{2}$$

where f_i is the channel frequency, c is a constant value representing the speed of light, and $\sigma_i = \sigma_T + \sigma_R + \sigma_{Tag}$ is the hardware induced phase offset on channel frequency f_i.

From (2), it can be seen that the phase offset has a big effect on the received signal. Fig. 1 presents the received signal from an RFID tag that contains such substantial noise that it is impossible to extract the target information directly from the signal. Recently, the problem of frequency hopping has been studied and a calibration method based on the reference channel has been proposed [15]. When calibrating a multi-channel signal, researchers often employ a reference channel approach to maintain phase coherence across frequency

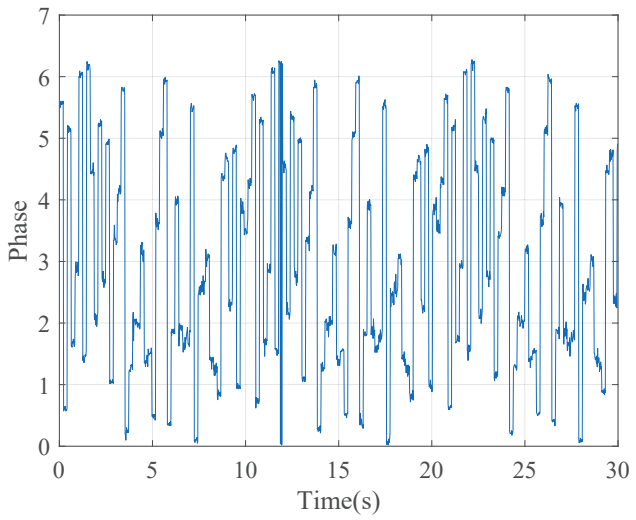

Fig. 1. Measured raw RFID phase data.

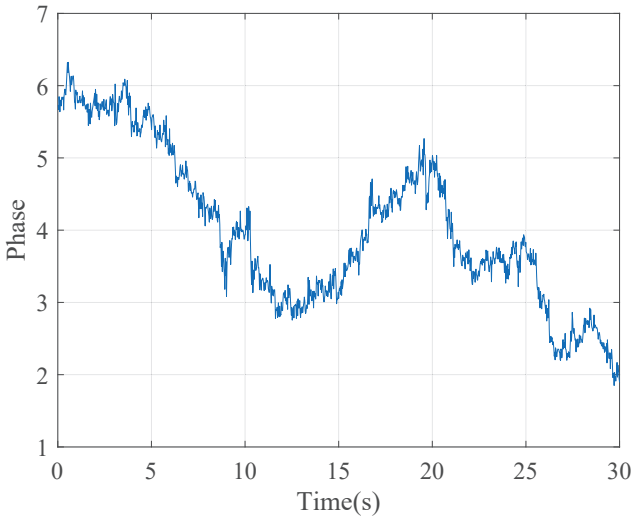

Fig. 2. The AutoTag method for calibration of the raw RFID phase data [15].

changes. The methodology involves the following steps. First, one of the channels is designated as the reference channel. Then, as the frequency switches from one channel to the next, a small set of phase values are recorded from the previous channel frequency, and a small set of the first phase values from the current channel frequency are recorded as well. Next, these two sets of phase values are averaged separately, and the phase difference between the averaged values from the previous and current channel frequencies is calculated. This phase difference is then used as the phase offset caused by the current frequency hopping. By applying this phase offset, the phase information across all channels can be converted to be around the reference frequency, effectively calibrating the signal. This technique allows effectively preserve the phase relationship between channels despite changes in the operating frequency, thus ensuring the integrity of the overall signal during analysis and processing.

Fig. 2 shows the calibrated phase data corresponding to that in Fig. 1 and calibrated with the AutoTag method [15]. It can be observed that this method does remove most of the noise compared to the original signal. However, it does not completely eliminate the phase error by simply calculating the mean. The residual error may still cause the signal to lose some of its useful information. In order to better mitigate the frequency hopping effect, we propose a new method in the proposed RFID system, to remove the phase offset σ_i, which will be discussed in Section III.

B. Contact-free Heartbeat Monitoring

The normal heart rate for a healthy adult at rest is $50 \sim 90$ beats per minute (bpm) [10], while the contraction and diastole of the heartbeat are not done uniformly in each frequency cycle. The spike waveform in the ECG is caused by the rapid contraction and diastole of the heart. With each heartbeat, the chest movements cause a small rise and fall trend. As shown in Fig. 3, the heart's movement generates a continuous wave that is captured by RFID signals and backscattered to the RFID reader [16]. Simultaneously, the chest's movements due to respiration also affect the RF signals, known as the moving effect of the tag pair. Consequently, the RFID reader receives a composite signal comprising the heartbeat, respiration, and ambient noise.

In order to better show how to extract the reflection signal of heartbeat from the received RFID signal, we introduce a signal propagation model to help explain the principle as illustrated in Fig. 3. The model uses two RFID tags: a reference tag and the target tag. We use A, T, R and H to indicate the locations of antenna, target tag, reference tag, and heart, respectively. As the target tag is attached on the test subject's chest, it will move in response to heartbeats, as well as breathing and body movements. In Fig. 3, d is used to represent the *distance change* caused by contraction and diastole of the heart, and the displacement positions of the target tag and heart are denoted as T' and H', respectively. The angle formed by the reflected signals at location T and T' and the horizontal ground is denoted as α and β, respectively. The antenna transmits a continuous radio wave to activate the tags. Due to the movement of heart, the round-trip diatance of the LOS path S_r will be time varying which can be expressed as

$$S_r = S_{AT} + S_{TA}, \tag{3}$$
$$S'_r = S_{AT'} + S_{T'A}, \tag{4}$$
$$S_{TA} = D_{TA} \cos\alpha, \tag{5}$$
$$S_{T'A} = D_{T'A} \cos\beta, \tag{6}$$
$$D_{T'A} \approx d + D_{TA}, \tag{7}$$

where S_{AT} is the distance from the antenna to the target tag, S_{TA} is the distance from the target tag to antenna, S'_r is the round-trip distance of the LOS path between the antenna and target tag at location T', and D_{TA} ($D_{T'A}$) is the horizontal

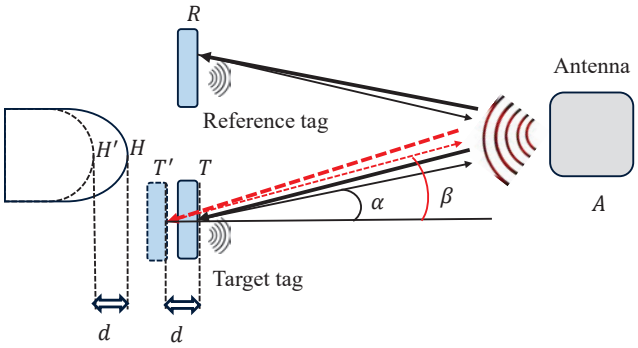

Fig. 3. Movement model of heartbeat induced tag displacements.

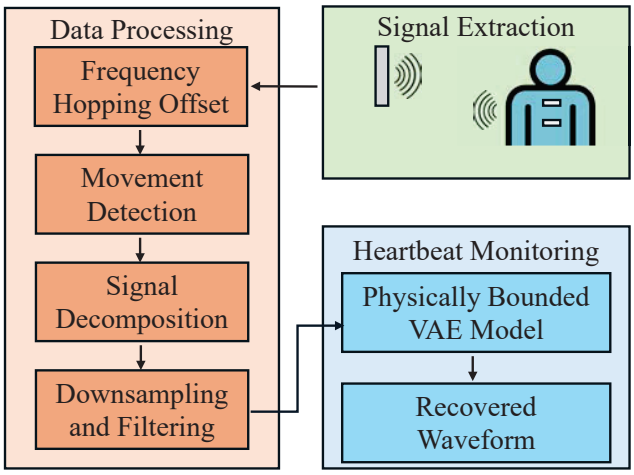

Fig. 4. The heartbeat detection RFID system design.

distance between the antenna and target tag at location T (T'). Since D_{TA} is much larger than d, we can simplify the formula into the following form:

$$S'_r = S_r + 2d. \tag{8}$$

Eq. (8) indicates that we can obtain the heartbeat frequency from the displacement variations of the target tag. Since the reference tag is attached on the collarbone of the test subject, the displacement of the reference tag can be ignored. We could subtract the reflected signal of the tag pair to obtain the displacement changes in the target tag.

III. System Design

The RFID system is designed to monitor human heartbeat and recover the waveform of the heartbeat using two RFID tags attached to the test subject. As shown in Fig. 4, the phase information collected by an RFID reader is a function of the distance between the corresponding tag and the reader antenna. The proposed system can be divided into three parts: signal extraction data processing, and heartbeat monitoring, which will be elaborated on in the remainder of this section.

A. Signal Extraction

The signal extraction module consists of RFID tags, an RFID reader, an antenna, and a computer. When tags are attached to the human body, its distance to the antenna changes periodically following the chest movement caused by the subject's breathing and heartbeat. As mentioned in Section II, we can leverage the RFID phase information to recover the periodic signal of heartbeat.

The low-level data from the tags shall be collected during breathing and heartbeats, while the data contains both chest and abdomen movements. It is not easy to directly obtain any useful information from the raw data. To increase the robustness of the system, we attach two passive RFID tags on the upper body of the subject. One is on the subject's chest, and the other is on the collarbone. The reader uses a special antenna to interrogate the tags. The data collected from the reflected signals from these tags includes phase, received signal strength indicator (RSSI), Doppler shift, and time stamp. The signals can capture the breathing and heartbeat patterns. However, correctly detecting heartbeat through RSSI and Doppler shift is not easy. This is because that RSSI lacks precision, and Doppler shift is not sufficiently reliable due to the slow movements of the subject's chest while breathing. As a result, the proposed system mainly leverages phase information to monitor heartbeat.

B. Data Processing

Fig. 1 illustrates the raw phase data collected from a tag over an interval of 30 seconds. It is observed that significant fluctuations are present in the phase data as the system cycles through different channels, spending 0.2 seconds on each channel. Furthermore, the phase data does not transition smoothly from one channel to another but rather changes abruptly. Consequentially, it is quite difficult to directly derive the heatbeat signal from received phase data. For a successful extraction of the breathing signal, it is required to pre-process the raw phase data as described in the following steps.

1) Frequency Hopping Offset: The output of phase data ranges from 0 to 2π. Because the tag movements are always continuous in time, two consecutive phase samples usually do not change by more than π. In the actual experiment, the phase can change from 0.1π to -0.1π over the previous sample, but the corresponding phase information at the output becomes 0.1π and 1.9π due to the modulo operation. Thus, we unwrap the phase data to remove the modulo operation.

However, unwrapping cannot completely solve the frequency hopping problem, because it can only be used for consecutive phase samples collected from the same channel. In order to mitigate the frequency hopping effect, we propose to use two RFID tags as a pair. Both tags are of the same type. One is attached on the chest, and the other to a location that hardly ever changes. Since the sampling rate of the reader is higher than 100 Hz, and the reader remains on each channel for up to 200 ms, we can guarantee that the channel frequency received by each tag is the same. From (2), we have

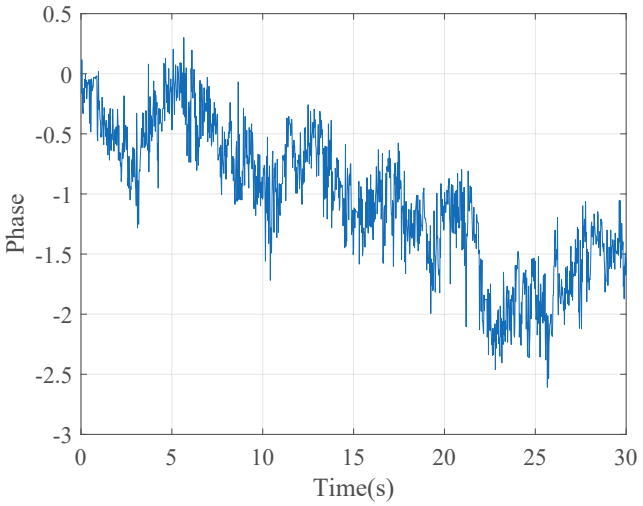

Fig. 5. Phase difference between the pair of RFID tags.

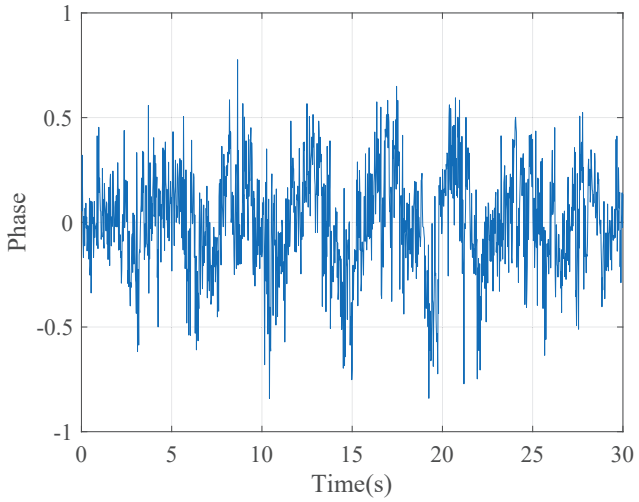

Fig. 6. The calibrated phase signal after removing the DC component.

demonstrated that the factors affecting the phase information are determined by the channel frequency, and that different channel frequencies result in different frequencies of reflected waves from the tag, as determined by the structure of the tag itself. Therefore, the same channel frequency can result in the same phase offset σ_i. Fig. 5 illustrates the result of our proposed method. The phase information in Fig. 5 contains much clearer waveform data compared to the method shown in Fig. 2.

2) Movement Detection: Either in Fig. 2 or Fig. 5, we can see that the human body has a small displacement during the experiment, which also causes a phase change. Since our target signal is the relatively much weaker heartbeat, avoiding the interference introduced by the relatively larger movements of human body is necessary.

Traditional methods usually utilize a sliding window to mitigate the impact of human body movement. For each window, the mean absolute deviation of the phase samples from all tags will be calculated. If the subject is not stationary, the phase values will exhibit large variations. Therefore, by setting a threshold of 0.9, the human body movement can be detected if the mean absolute deviation is larger than the threshold value.

In our proposed method, we attach the reference tag on the collarbone for two reasons. First, the collarbone is relative more stationary and is virtually unaffected by the movement of the chest. Second, the tag pair can form a relative coordinate system. The tags move with the body movement. The phase difference can be considered as a function of the distance of the target tag with respect to the reference tag. Thereby, we can effectively mitigate errors caused by body movement by using the phase difference.

Although the frequency hopping offset can be effectively mitigated by using phase difference, the initial phase offset is still a random value that introduces a random DC component in the phase data. To remove the random DC component, we utilize a polynomial to fit the resulting phase information and then subtract the predicted phase information from the collected samples, thus calibrating the phase data. The calibrated signal is plotted in Fig. 6. It can be seen that the calibrated signal is now centered at zero and the breathing cycles are also more obviously visible.

3) Signal Decomposition: After mitigating the frequency hopping offset and calibrating the phase information, the phase data mainly contains three types of information, i.e., respiration, heartbeat, and noise, the first two of which are more dominant and have different frequency ranges for subjects. The respiration signal contains the most energy. In contrast, heartbeat signals are mixed with noise signals, which are difficult to distinguish and only approximate frequency ranges could be obtained from some fluctuations. It can be observed in Fig. 7 for the reported phase with fast Fourier transform (FFT) from one experiment. In order to separate the heartbeat signal from the phase data, a signal decomposition method is implemented to achieve this goal.

The frequency range of respiration and heartbeat are mainly within $0.1 \sim 0.5$ Hz and $0.8 \sim 2.5$ Hz, respectively. The peak in the frequency domain of these signals can be regarded as the coarse respiration rate or heartbeat rate. In this module, the EMD approach is leveraged to extract the heartbeat frequency from the phase information. EMD is based on data, and does not require a pre-set mother wavelet. It is also a type of blind source separation (BSS) technique, which means that EMD operates effectively even when there are more source signals than the recorded signals. More importantly, EMD is a process that decomposes a signal into components known as intrinsic mode functions (IMF), along with a trend. The key advantage of EMD is that it operates well with data that is constantly changing and does not follow a linear pattern. This is because EMD operates based on the local, specific time scale of the data, ensuring that the changing frequency characteristics are preserved [17].

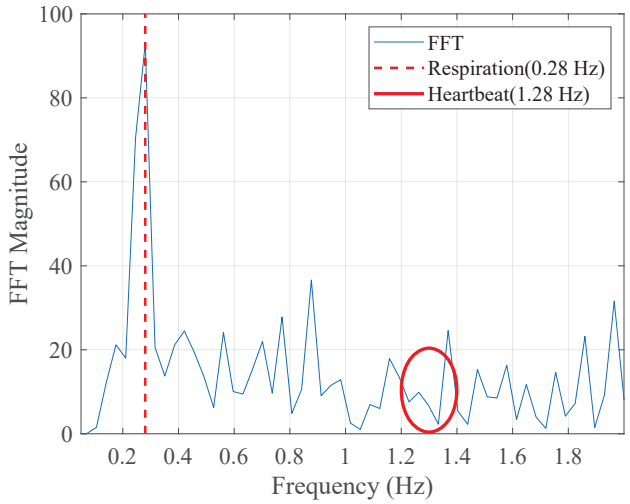

Fig. 7. FFT of reported phase in one experiment. The vertical line and the circle indicate the ground truth respiration and heart rate, respectively.

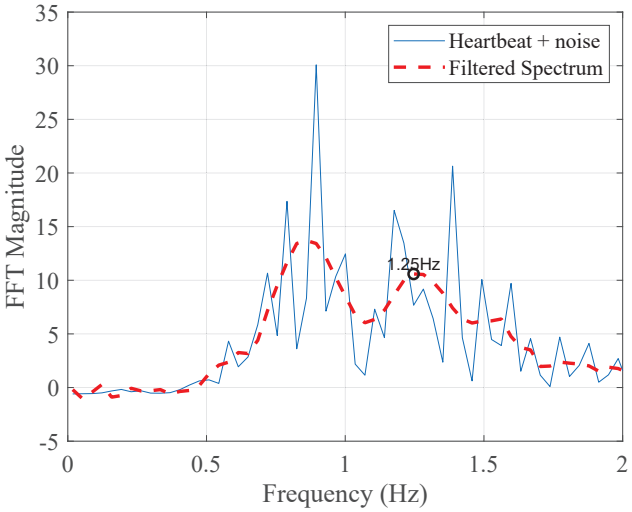

Fig. 8. Filtered spectrum and target frequency.

As the order of the IMF gets higher, the related signal frequency drops. We can estimate the strength and frequency of each IMF through the Hilbert Transform. The decomposition process can stop once the frequency of an IMF falls below the threshold frequency of either the breathing or heartbeat signal. The IMF corresponding to respiration and heartbeat are usually the two strongest ones while others represent noise. The respiratory signal is not significantly affected by noise because the respiratory frequency has most of the energy compared to other signals (i.e., the strongest component). However, during our attempt to isolate the heartbeat signal, we find that the harmonic waves and background noise make it difficult to clearly distinguish the heartbeat signal within the decomposed component of the IMF signal.

In order to achieve our target, we first obtain the spectral distribution of the compound signal. Next, we identify the IMF signal that possesses the highest energy, which is considered as the breathing signal's spectrum. Then we obtain the spectral distribution of the heartbeat signal and part of noise signal by subtracting the spectrum of the breathing signal from the overall signal. Due to the presence of harmonics, the spectrum we obtain still shows high amplitude at the breathing-induced frequencies. To address this issue, we adjust our target frequency domain to the range of $0.8 \sim 2.5$ Hz. We then reduce the signal to its average value, making the signal symmetrical around zero. To minimize noise interference, we employ a Savitzky-Golay filter to smooth the spectrum. We then disregard the most prominent peak frequency, opting instead for the second peak. This is because the third harmonic related to breathing is stronger than the heartbeat signal. We then identify the frequency through this method as the central heartbeat signal frequency. We choose the frequency interval to be within $\pm$ 0.1 Hz of this central frequency.

The signal decomposition is illustrated in Fig. 8. The solid line represents the residual spectrum, obtained by subtracting the domain frequency spectrum from the original phase signal. The dotted line, on the other hand, represents the spectrum that has been processed through the Savitzky-Golay filter. Notably, there are two distinct peaks that present in the curve. The first peak is influenced by the breathing signal. Our target frequency, however, is indicated by the second peak. In this specific experiment, the target frequency sits at 1.25 Hz. It is important to note that there is a slight frequency shift from the ground truth of 1.28 Hz in this experiment.

4) Downsampling and Filtering: After the range of heartbeat rate is determined, we employ the Butterworth filter to extract the heartbeat signal from the phase information. The result is shown in Fig. 9. Due to the filtering performed, the spectrum of the obtained signal is not exactly the same as the ground truth, as can be seen in Fig. 8, where the wave peaks of the estimated signal and the ground truth are not exactly identical. Nevertheless, it is noted that the extracted signal basically achieves peak alignment compared to the ground truth, verifying the accuracy of the extracted heartbeat signal. The relative error of the distance between heartbeats, also known as the RR interval, which is commonly used in medicine, is also less than 2%. To better match the data from the ground truth, the obtained data needs to be downsampled with a sampling frequency of 50 Hz.

C. Heartbeat Monitoring

Simply obtaining the frequency of the heartbeat signal does not yield sufficient useful information for some practical applications. As mentioned in the last subsection, the estimated signal only shows the heart rate, but without other critical information. In this study, we utilize the method of deep learning to obtain the heartbeat waveform. In this subsection, we first motivate our approach and introduce the VAE model to be adopted, followed by presenting the modified loss function with physical boundaries as well as the rationale of the enhanced loss function.

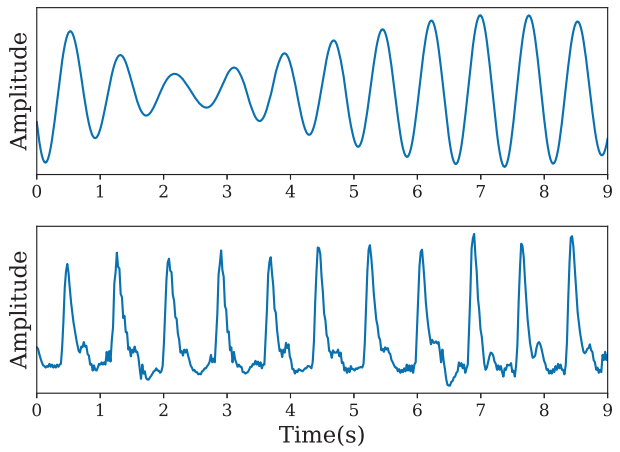

Fig. 9. Signal decomposition result (top subfigure) vs. the ECG ground truth (lower subfigure).

1) VAE Model: In order to recover the waveform of the heartbeat signal, a VAE model is adopted in our proposed system. First, we clarify why we select the proposed method and present the rationale behind our VAE model's design. Then we provide a brief overview of its structure, followed by an exploration of the functionality and training process of each component. The goal is to offer a clear understanding of our method and its individual parts.

Essentially, obtaining the heartbeat waveform from the RF signal is like creating a model that represents the conditional distribution of the heartbeat waveform, which relies on the phase information. These methods, which are motivated by raw RF signals and actual waveform data, can automatically identify the complex relationship between the input and output. A recent example of this method is to learn this relationship through deep neural networks [8].

In our model shown in Fig. 10, the encoder learns the feature from the input data and encodes it into a latent space structure. The internal structure of the multidimensional latent space for a well-learned model defines its properties. The decoder component then reconstructs the input using this information. The key idea of VAE is to compress a random vector x in a high-dimensional space into a latent variable z in a low-dimensional space by variational encoding. This process can be simplified and expressed as follows:

$$P_\theta(x, z) = P_\theta(x|z)P_\theta(z), \tag{9}$$

where $P_\theta(z)$ denotes the prior distribution of the latent variable z, which is generally set to the standard Gaussian distribution; $P_\theta(x|z)$ denotes the conditional probability density function of the input variable x when z is known; and θ denotes the variable parameter. The posterior distribution $P_\theta(z|x)$ is intractable since the parameters θ and the latent variable z are unknown. The standard VAE uses a recognition model $q_\phi(z|x)$ as an approximation to the true posterior $P_\theta(z|x)$. VAE generates two outputs in the encoder including a mean

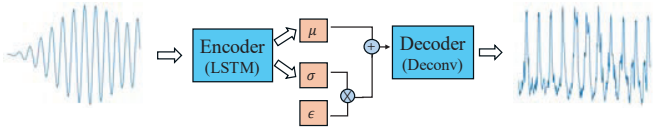

Fig. 10. The architecture of the VAE model used in our system. The encoder takes processed phase data and encodes it to respective latent probability distributions. Latent vectors are then sampled from the distributions and fed to the decoder for recovering the heartbeat waveform.

vector and a standard deviation vector. These two vectors form the parameters of the latent variable z. This mechanism allows the encoder to learn different mean values corresponding to each potential class, and the standard deviation reduces the overlap of feature classes.

2) Loss Function Based on Physical Boundaries: The commonly used loss function in the VAE model is a combination of reconstruction loss (l_r) and the Kullback-Leibler (KL) divergence (l_k). However, this loss function ignores the physical boundaries in practical applications. The experimental data of the target have distinctive features, and each set of data has a relatively fixed peak-to-peak spacing as well as the number of wave crests. While the commonly used loss functions do not take such physical characteristics into account, we propose an enhanced loss function to improve the overall performance of the model by incorporating physical boundaries.

Algorithm 1 Loss Function Based on Physical Boundaries Algorithm

Require: $Target$, $Input$, μ, σ
Calculate $\nabla Target$
$Target\_gradients \leftarrow \nabla Target_{Max}[0:25]$
for each i in index **do**
  Get neighborhood of i from $Target\_gradients$ with sample points N
  max_value $\leftarrow$ maximum value in the neighborhood
  if max_value is not in peaks **then**
    Append max_value to peaks
    Append i to locations
  end if
end for
Sort $locations$
$\overline{distance} \leftarrow \sum diff(locations)/(num(peaks)-1)$
Calculate $std(peaks)$ and $num(peaks)$
$repeat$ 1-13 with $Input$
Compute $gradient\_loss$ as the sum of MSE losses of $\overline{distance}$, $std(peaks)$, and $num(peaks)$ of input and target
Compute VAE_loss by calling VAE loss function with $Target$, $Input$, μ, and σ
$total\_loss = \omega_1 \cdot gradient\_loss + \omega_2 \cdot VAE\_loss$
return $total\_loss$

Our loss function can be obtained through Algorithm 1, where $Target$ is the ground truth data, $Input$ is the phase information; μ and σ are the mean value and standard variance

of value x, respectively. They are calculated by encoder $e_\theta(x)$. ∇ means the gradients of the data. N is the sample points which depends on the sampling rate. $\overline{distance}$ is the mean value of the distance of the RR waves. $std(peaks)$ means the standard deviation of the heartbeat peaks. ω_1 and ω_2 are the weights used in the loss function. In Algorithm 1, we first find the possible heartbeat peaks by calculating the gradient of the input data, and then obtain the exact heartbeat peaks and the corresponding indices by finding the local maxima. Furthermore, we can calculate the RR interval as well as the number of heartbeat peaks for the corresponding data. After calculating the physical values, we can use these parameters to constrain the loss function, enabling it to produce results that more closely align with the characteristics of the target data.

IV. Experimental Study

In this section, we evaluate the performance of the proposed system, and in particular, assess the enhanced VAE model's ability to recreate the pattern of heartbeat across various real-world scenarios and settings.

A. Evaluation Setup

Our experiment is extensively evaluated in an office with varying parameter settings. To obtain the ground truth of the heartbeat signal, the Neulog NUL 208 and Heal Force Prince $180B$ devices are applied. Each experiment lasts one minute. The sampling rate of the RFID reader is about 50 Hz. During the experiment, the volunteer remains to be still. The two tags that make up the tag pair are attached to the chest and collarbone regions, respectively, which are 10 cm apart. To better understand the performance of the proposed system under various conditions, we conduct measurements when the test subjects sit at different distances from the antenna. Because for each test, the ground truth lasts for 30 seconds, to ensure that the ground truth can cover the collected RFID data, we split the data into 9-second segments.

We compare the proposed method with an ensemble EMD (EEMD) method that is a state-of-the-art signal decomposition method [8], [18]. To numerically measure the quality of the waveform reconstruction, we employ cosine similarity and relative error as the metrics.

B. Overall Performance Results

To visualize the quality of our proposed signal recovery method, we compare the recovered data alongside the ground truth, and the results are shown in Fig. 11. The cosine similarity of the two curves is 0.9118 and the relative error is within 2%. Evidently, the recovered signal has a similar trend as the ground truth and the portion of the waveform that does not match can also be inferred as the location of the T-wave.

We have further analyzed our findings using the previously mentioned metrics, resulting in a more detailed evaluation. The results, as shown in Fig. 12, demonstrate that our proposed method consistently produces a median cosine similarity that exceeds 0.83 for the RFID signal. On the other hand, the benchmark approach only achieves a median cosine similarity value of 0.70.

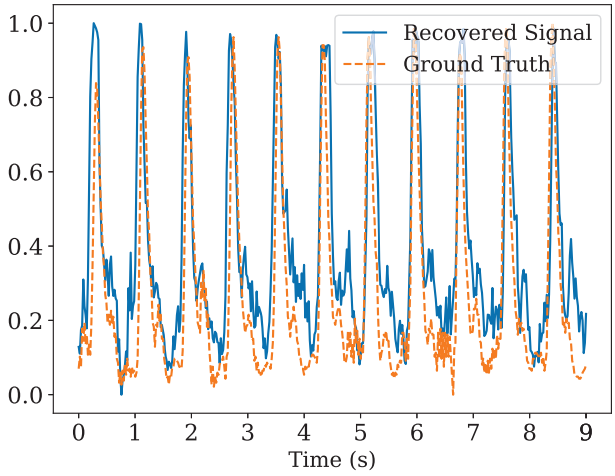

Fig. 11. Examples of the heartbeat waveform recovered from the RF signal.

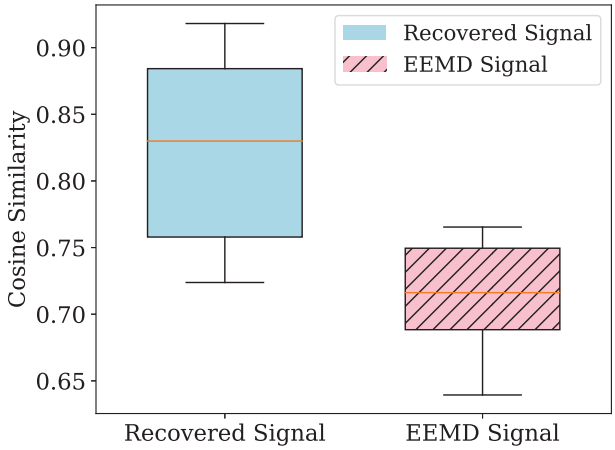

Fig. 12. Comparing the cosine similarity of recovered signal with baseline.

An analysis of heart rate estimates shown in Fig. 13 also highlights the performance of our proposed method. It shows median errors of less than 3%, a considerable improvement over the baseline method, which achieves median errors around 8%, while the peak errors climbing up to 15%. While the baseline may be sufficient for some applications, our method is clearly more desirable owing to its high-accuracy heartbeat waveforms. This makes it more capable of handling complex and varied application scenarios, thereby surpassing the baseline method across all assessment metrics.

C. Impact of Practical Factors

In the following, we study the impact of different sensing distances, while focusing on evaluating the cosine similarity that measures the overall performance of waveform recovery. We control the distance between the tags and antenna to be 0.25 m, 0.5 m, 0.75 m, and 1 m, respectively. The cosine

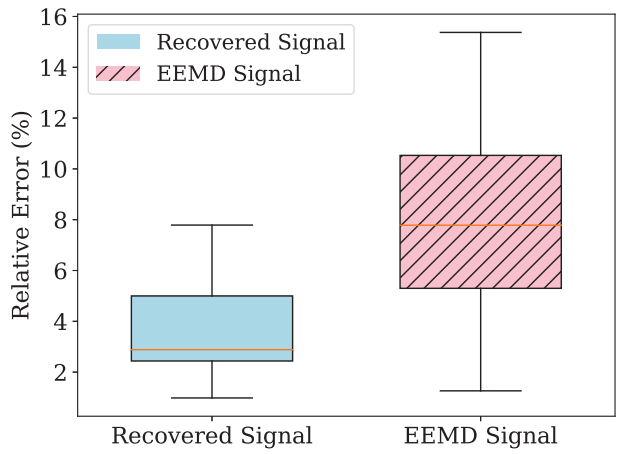

Fig. 13. Comparing the relative error of recovered signal with baseline.

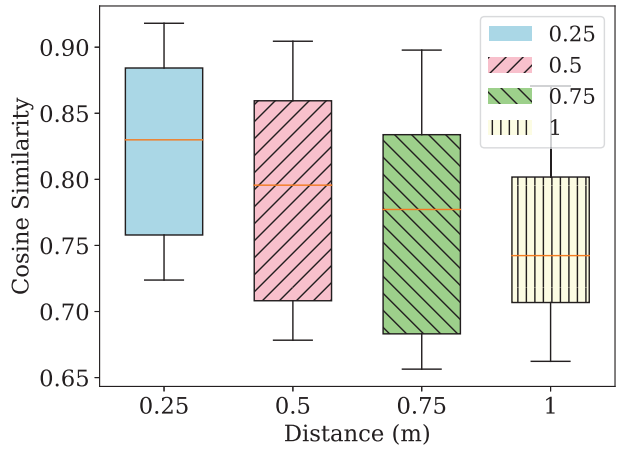

Fig. 14. Impact of different sensing distances.

similarity results in Fig. 14 indicate that the distance between the RFID tags and antenna does influence the performance of the system. As the distance is increased, the results become worse and more discrete. This is because the reflected signal becomes weaker for increased distances. However, the results are still better than the baseline, and the median cosine similarity is still above 0.70 under our test scenario.

V. Conclusion

In this paper, we designed a contactless and low-cost heartbeat monitoring system with COTS RFID devices. The system employed a sequence of signal processing techniques to accurately estimate the heartbeat signal, taking into account the derived phase information, and mitigating the noise and body movement impacts. After extraction, these signals served as input to the enhanced VAE model to recover the heartbeat waveform. The results demonstrated that the proposed method was reliable and robust. Our proposed method achieves a high performance with median relative error below 3% and median cosine similarity above 0.83 in the device-free scenario.

Acknowledgment

This work is supported in part by the US NSF under Grants IIS-2306789, IIS-2306790, IIS-2306791, and IIS-2306792.

References

[1] F. Kawsar, C. Min, A. Mathur, A. Montanari, U. G. Acer, and M. Van den Broeck, "eSense: Open earable platform for human sensing," in *Proc. ACM UbiComp 2018*, Singapore, Oct. 2018, pp. 371–372.

[2] D. T. Martin, M. M. Bersohn, A. L. Waldo, M. S. Wathen, W. K. Choucair, G. Y. Lip, J. Ip, R. Holcomb, J. G. Akar, and J. L. Halperin, "Randomized trial of atrial arrhythmia monitoring to guide anticoagulation in patients with implanted defibrillator and cardiac resynchronization devices," *European Heart J.*, vol. 36, no. 26, pp. 1660–1668, July 2015.

[3] C. Xu, H. Li, Z. Li, H. Zhang, A. S. Rathore, X. Chen, K. Wang, M.-C. Huang, and W. Xu, "Cardiacwave: A mmwave-based scheme of non-contact and high-definition heart activity computing," *Proceedings of the ACM on Interactive, Mobile, Wearable and Ubiquitous Technologies*, vol. 5, no. 3, pp. 1–26, Sept. 2021.

[4] X. Wang, C. Yang, and S. Mao, "On CSI-based vital sign monitoring using commodity WiFi," *ACM Transactions on Computing for Healthcare*, vol. 1, no. 3, pp. 12:1–12:27, Apr. 2020.

[5] X. Fan, D. Pearl, R. Howard, L. Shangguan, and T. Thormundsson, "APG: Audioplethysmography for cardiac monitoring in hearables," in *Proc. ACM MobiCom 2023*, Madrid, Spain, Oct. 2023, pp. 1–15.

[6] A. Vilesov, P. Chari, A. Armouti, A. B. Harish, K. Kulkarni, A. Deoghare, L. Jalilian, and A. Kadambi, "Blending camera and 77 Ghz radar sensing for equitable, robust plethysmography," *ACM Trans. Graph.*, vol. 41, no. 4, pp. 36:1–36:14, July 2022.

[7] Z. Wang, B. Jin, S. Li, F. Zhang, and W. Zhang, "ECG-grained cardiac monitoring using uwb signals," *Proceedings of the ACM on Interactive, Mobile, Wearable and Ubiquitous Technologies*, vol. 6, no. 4, pp. 1–25, Jan. 2023.

[8] S. Zhang, T. Zheng, Z. Chen, and J. Luo, "Can we obtain fine-grained heartbeat waveform via contact-free rf-sensing?" in *Proc. IEEE INFOCOM 2022*, London, UK, May 2022, pp. 1759–1768.

[9] O. Kaltiokallio, H. Yiğitler, R. Jäntti, and N. Patwari, "Non-invasive respiration rate monitoring using a single COTS TX-RX pair," in *Proc. IEEE IPSN 2014*, Berlin, Germany, Apr. 2014, pp. 59–69.

[10] J. W. Mason, D. J. Ramseth, D. O. Chanter, T. E. Moon, D. B. Goodman, and B. Mendzelevski, "Electrocardiographic reference ranges derived from 79,743 ambulatory subjects," *Elsevier Journal of Electrocardiology*, vol. 40, no. 3, pp. 228–234, May-June 2007.

[11] R. Zhao, D. Wang, Q. Zhang, H. Chen, and A. Huang, "CRH: A contactless respiration and heartbeat monitoring system with COTS RFID tags," in *Proc. IEEE SECON 2018*, Hong Kong, China, June 2018, pp. 1–9.

[12] C. Wang, L. Xie, W. Wang, Y. Chen, Y. Bu, and S. Lu, "Rf-ecg: Heart rate variability assessment based on cots rfid tag array," *Proceedings of the ACM on Interactive, Mobile, Wearable and Ubiquitous Technologies*, vol. 2, no. 2, pp. 1–26, July 2018.

[13] Z. Chen, T. Zheng, C. Cai, and J. Luo, "MoVi-Fi: Motion-robust vital signs waveform recovery via deep interpreted RF sensing," in *Proc. ACM MobiCom 2021*, New Orleans, LA, Mar.-Apr. 2021, pp. 392–405.

[14] Impinj, "Low level user data support," Impinj Speedway Revolution Reader Application, 2013.

[15] C. Yang, X. Wang, and S. Mao, "Unsupervised detection of apnea using commodity RFID tags with a recurrent variational autoencoder," *IEEE Access Journal*, vol. 7, no. 1, pp. 67 526–67 538, June 2019.

[16] L. Yang, Q. Lin, X. Li, T. Liu, and Y. Liu, "See through walls with COTS RFID system!" in *Proc. ACM MobiCom 2015*, Paris, France, Sept. 2015, pp. 487–499.

[17] N. E. Huang, Z. Shen, S. R. Long, M. C. Wu, H. H. Shih, Q. Zheng, N.-C. Yen, C. C. Tung, and H. H. Liu, "The empirical mode decomposition and the hilbert spectrum for nonlinear and non-stationary time series analysis," *Proceedings of the Royal Society of London. Series A: mathematical, physical and engineering sciences*, vol. 454, no. 1971, pp. 903–995, Mar. 1998.

[18] W. Hu, Z. Zhao, Y. Wang, H. Zhang, and F. Lin, "Noncontact accurate measurement of cardiopulmonary activity using a compact quadrature doppler radar sensor," *IEEE Transactions on Biomedical Engineering*, vol. 61, no. 3, pp. 725–735, Mar. 2013.